DEUTSCHES ELEKTRONEN-SYNCHROTRON DESY

DESY 74/12
April 1974

A New Approach to Evaluate Sputter-Ion Pump Characteristics

by

H. Hartwig and J. Kouptsidis

2 HAMBURG 52 · NOTKESTIEG 1

To be sure that your preprints are promptly included in the
HIGH ENERGY PHYSICS INDEX ,
send them to the following address (if possible by air mail) :

DESY
Bibliothek
2 Hamburg 52
Notkestieg 1
Germany

A NEW APPROACH TO EVALUATE SPUTTER-ION PUMP CHARACTERISTICS

by

H. Hartwig and J. Kouptsidis

By using theoretical considerations combined with experimental results a general approach to evaluate sputter-ion pump characteristics is given. This approach can be successfully applied to optimal design of distributed sputter-ion pumps in high energy accelerators. The agreement between proposed and measured pumping speed values is better than 30 %.

Introduction

Despite the widespread use of sputter-ion pumps in almost all vacuum applications, our knowledge about the influence of the different pump parameters on the pumping speed is more empirical than fundamental.

This is probably due to the complicated pumping mechanism of the sputter-ion pumps, which depends on the different discharge modes of the Penning cells, on the sputtering rate of the energetical ions impacting the cathode, and on physicochemical phenomena between gas molecules and the surfaces of both electrodes.

Besides the cathode material, the main significant parameters affecting the pumping speed of a sputter-ion pump are the magnetic field, the applied voltage and the diameter of the cells. Fortunately for the designers of conventional sputter-ion pumps, the values of the magnetic field and the voltage are cost limited and can not be optimized. Almost all pumps work with magnetic fields of 1-2 kG and voltages of 5-8 kV. The remaining parameter, the cell diameter, can be optimized experimentally.

Recently, the sputter-ion pumps have been found another application in particle accelerators, particulary in storage rings [1,2,3] as distributed pumping units. The bending magnets of the particle accelerators provide the magnetic field required for the pump. The magnetic field of the bending magnets of a storage ring is proportional to the energy of the stored electrons and generally ranges between 0,5 and 12 kG [4].

In the case of electron storage rings the gas desorption of the vacuum system is due mainly to the synchrotron radiation which depends on the energy and current of the stored electrons [5]. Thus the distributed sputter-ion pumps for a storage ring must be designed to perform optimally when the maximum gas desorption takes place in the accelerator. It must also provide a sufficiently large pumping speed over the whole operating range of the accelerator.

Unfortunately the only empirical formalism of M.D. Malev et al.[1,21] for optimal design of sputter-ion pumps shows discrepancies between measured and expected pumping speed when the magnetic field varies.

Fig.1 shows these discrepancies as observed for prototypes of distributed pumps of the SPEAR storage ring[2]. For these large cells (Ø 2,5 cm), working in high magnetic fields (> 10 kG) the deviation between calculated and measured pumping speed goes up to a factor of 5.

In contrast to Malev's formalism, it is well-known that the pumping speed of a sputter-ion pump reaches a limit value when the magnetic field is increased. This limit is not due to the conductance of the pump elements, but it is an inherent property of the Penning discharge [6].

Malev's formalism is an empirical result from pumping speed measurements made over a broad range of values of cell parameters such as diameter, applied voltage and magnetic field. While making these large variations, the discharge takes place in different modes, and the measured pumping speed values can not be fitted by an empirical formalism without a classification in these modes. The different discharge modes and errors in the pumping speed measurements probably explain the observed discrepancies.

In this paper a new semiempirical formalism to determine the characteristics of sputter-ion-pumps is proposed. This formalism uses existing theories of the different discharge modes of a Penning cell [6] combined with experimental results on the pumping speed of sputter-ion pumps obtained at DESY and other laboratories [2,6,7].

Pumping speed and discharge intensity

In the early works on sputter-ion pumps it was suggested and experimentally proved that the pumping speed is closely related to discharge intensity I/P (I = discharge current, P = pressure)[7,8,9,10,11]. This relationship is linear ($S = c \frac{I}{P}$) for a given gas and was used to determine the pumping speed especially at low pressures since the discharge intensity can easily be measured.

The proportionality factor c depends not only on the gas but also on the gas quantity pumped after bake out of the pump. To avoid complications due to such saturation effects, we first deal with pumping speeds of virgin pumps after appropriate bake-out.

The two extreme published c-values for nitrogen [7,9,10,11] vary by factors as high as 3 (0,027 - 0,08 Torr·lit/secA). This probably due to the inherent incertitude of absolute pressure measurement at high pumping speeds, where non-equilibrium conditions occur.

Pumping speed measurements on different conventional pumps, carried out at DESY according to a proposal from E. Fischer and H. Mommsen [12], give the best fit for a value of c = 0,075 Torr·lit/sec·A. This value is nearly the same as measured by Bächler [7] and lies between the two values 0,05 and 0,08 Torr·lit/sec·A assumed by Rutherford [9], seriously deviating only from the low value of 0,027 as estimated by Dallos et al. [10,11]. At pressures higher than 10^{-7}Torr the surface coverage of the electrodes increases resulting in a decrease of the effective pumping speed by electron and ion impact desorption.This can be taken into account using the empirical relation $c = 0{,}075 \left(1 - \frac{1{,}5 \cdot 10^6 p}{1+4 \cdot 10^6 p}\right)$.

The equation:

$$S = 0{,}075 \left(1 - \frac{1{,}5 \cdot 10^6 p}{1+4 \cdot 10^6 p}\right) \frac{I}{p}$$

where

S = the pumping speed in lit/sec.,

$\frac{I}{p}$ = the discharge intensity in A/Torr,

is the base of the semiempirical formalism. The constants and the following calculations are valid only for nitrogen.

Existing theories on the different discharge modes of a Penning cell given in Schuurman's survey [6] were used to calculate the discharge intensity.

Only two operation modes are significant for sputter-ion pumps working in the region of high and ultrahigh vacuum: the LMF-mode (Low-Magnetic-Field) and the HMF-mode (High-Magnetic-Field). These modes differ in their potential profile in the cell.

In the LMF-mode the potential profile in the cell is strongly deformed by the space charge of an electron cloud spread out over the whole volume of the cell. The

HMF-mode, existing at high magnetic fields, is characterized by a field-free plasma region around the axis of the cell and by a cloud of electrons in the form of a sheath adjacent to the anode.

The two modes can be easily distinguished in a typical diagram (Fig.2) which shows the dependence between the discharge intensity and the magnetic field at constant pressure.

At magnetic fields lower than the value A no ignition of the discharge takes place and the discharge intensity is zero. The ignition point A depends on the radius r_a of the anode cell and is given by the empirical equation:

$$B_i = \frac{300}{r_a} \qquad (2)$$

r_a = cell radius in cm

B_i = magnetic field at the ignition point in G.

This empirical equation is valid mainly for high working voltages (U_a > 3000Volts).

The branch AO (Fig.2) shows the typical increase of the discharge intensity with the magnetic field for the LMF-mode. The transition to the HMF-mode occurs where the discharge intensity has its maximum value (Point O).

At low pressures ($p < 10^{-7}$ Torr) the discharge intensity of the HMF-mode remains almost constant when the magnetic field is increased (branch OC). For $p > 10^{-7}$Torr the discharge intensity decreases (branch OD) with increasing magnetic field. This decrease is accelerated for higher pressure values.

The magnetic field B_{tr} at the transition point O between the LMF- and HMF-modes is given by the equation [6]:

$$B_{tr}^2 = 30{,}3 \frac{U_a}{r_a^2 \left(\frac{\nu_i}{\nu_c}\right)} \qquad (3)$$

U_a = applied voltage in V

r_a = cell radius in cm

B_{tr} in G.

$\frac{\nu_i}{\nu_c}$ is the ionisation probability of an electron in a collision with a gas molecule (ν_i = ionization frequency, ν_c = collision frequency).

The discharge intensity of one cell in the LMF-mode is given by the equation [6]:

$$\frac{J}{P} = 7{,}7 \cdot 10^{-4} \left(\frac{\nu_i}{\nu_c}\right)^2 \ell \, r_a^2 B^2 \qquad (4)$$

$\frac{J}{P}$ in A/Torr,

ℓ = effectiv height of the cell in cm, [×]

B = magnetic field in G.

This equation is valid only above the ignition point, i.e. for magnetic fields greater than B_i (Fig.2). To avoid discontinuity of the discharge intensity function at this point we take a linear rise starting at B_i and merging tangentially into the parabolic curve (eq. 4). Thus the LMF-mode between the magnetic fields B_i and $2B_i$ can be given by the linear equation:

$$\frac{J}{P} = 3{,}1 \cdot 10^{-3} \left(\frac{\nu_i}{\nu_c}\right)^2 \ell \, r_a^2 \, B_i (B - B_i) \qquad (5)$$

Equation (4) must be used to calculate this discharge intensity for magnetic fields greater than $2B_i$.

In order to reduce the computational effort to a minimum we have assumed that in the whole region of the HMF-mode the discharge intensity takes the transition point value. This assumption has been confirmed experimentally [6] for pressures below 10^{-7} torr. The deviation from this assumption at pressures higher than 10^{-7} torr is corrected by the empirical factor $\left(1 - \frac{1{,}5 \cdot 10^4 \cdot \sqrt{(B - B_{tr})\, r_a\, P}}{U_a}\right)$

Thus the following equation was assumed for the HMF-mode:

[×]) As effectiv height of the cell can be taken the height of the cell plus 25 % of the gap between anode and cathode (Fig. 5).

$$\frac{J}{P} = 2{,}3\cdot 10^{-2}\ \left(\frac{\nu_i}{\nu_c}\right)\ \ell\ U_a\ \left(1-\frac{1{,}5\cdot 10^4\sqrt{(B-B_{tr})\ r_a\ P}}{U_a}\right) \qquad (6)$$

It is well known [11] that the discharge current of a sputter ion pump is not proportional to the pressure, but rather a function of the type $k\cdot p^{\alpha}$ where the exponent α is slightly greater than 1. This typical dependence causes a decrease of the pumping speed at lower pressure. Thus the discharge intensity and the pumping speed show a pressure dependence of the type $k'p^{\alpha-1}$ [11]. The anomalous diffusion of the avalance electrons across the magnetic field - owing to colledtive interactions in the discharge - is mainly responsible for this dependence.

In order introduce this pressure dependence of the discharge intensity in equations (2), (3), (4), (5) and (6) - classical electron diffusion in the discharge - we assumed a pressure dependence of the ionization probability $\frac{\nu_i}{\nu_c}$. This assumption does not have any deep physical meaning ; it rather is a consequence of the attempt to consider the component of the anomalous diffusion of the discharge electrons by using theories of the classical electron mobility.

From measurements on different pumps working in LMF-mode over the whole pressure region, it has been found that the discharge current shows the following pressure dependence:

$$I \propto P^{1,2} \qquad (7)$$

Introducing this relation into the equation (4) results to a smooth pressure dependence of the ionization probability:

$$\frac{\nu_i}{\nu_c} \propto P^{0,1} \qquad (8)$$

By relating this dependence to pumping speed measurements it was possible to determine the proportionality factor in this equation:

$$\frac{\nu_i}{\nu_c} = 0{,}52\ \ P^{0,1} \qquad (9)$$

Equation (9) is plotted in Fig. 3 together with measured values of the ionization

probability given by Schuurman [6]. A good agreement between proposed and measured values of the ionization probability can be observed.

In practical cases the magnetic field lines are not parallel to the axis of the cell due to misalignment of the cell or to inhomogeneities of the magnetic field.

To calculate the influence of this misalignment we assume that the electrons of the discharge build up a cylindrical cloud along the magnetic field lines through the center of the cell. A misalignment angle of ϕ limits the electron cloud to a radius r_ϕ smaller than r_a (Fig.4).

From geometry the following relation results for r_ϕ:

$$r_\phi = r_a \cos\phi - \frac{\ell}{2} \sin\phi \qquad (10)$$

Using the effective radius of the cell in the equations (2), (3), (4), (5) and (6) it is easy to determine the influence of misaligment on the discharge intensity.

Summary of the formalism and numerical applications

The ignition of the discharge take place for magnetic fields greater than B_i:

$$B_i = \frac{300}{r_a} \qquad (11)$$

Transition to HMF-mode take place at:

$$B_{tr} = \frac{7{,}63\ \sqrt{U_a}}{r_a p^{0{,}05}} \qquad (12)$$

Nitrogen pumping speed of one cell:

1) LMF-mode $\quad B_i \leq B \leq 2B_i$,

$$S_l = 6{,}27 \cdot 10^{-5} \left(1 - \frac{1{,}5 \cdot 10^6 p}{1+4 \cdot 10^6 p}\right) p^{0{,}2}\ \ell r_a^2\ B_i (B - B_i) \qquad (13)$$

2) LMF-mode, $2B_i \leq B \leq B_{tr}$,

$$S_l = 1{,}56 \cdot 10^{-5} \left(1 - \frac{1{,}5 \cdot 10^6 p}{1+4 \cdot 10^6 p}\right) P^{0,2} \ell r_a^2 B^2 \qquad (14)$$

3) HMF-mode, $B \geq B_{tr}$,

$$S_l = 9{,}1 \cdot 10^{-4} \left(1 - \frac{1{,}5 \cdot 10^6 p}{1+4 \cdot 10^6 p}\right) P^{0,1} \ell U_a \left(1 - \frac{1{,}5 \cdot 10^4 \sqrt{(B-B_{tr}) r_a P}}{U_a}\right) \qquad (15)$$

Symbols and units:

- B = applied magnetic field in G,
- B_i = magnetic field at the ignition point in G,
- B_{tr} = magnetic field at the transition point in G,
- ℓ = effective height of the cell in cm,
- P = pressure in Torr,
- r_a = cell radius in cm,
- S_l = nitrogen pumping speed of one cell in lit/sec,
- U_a = anode voltage in V.

In an actual sputter-ion pump the pumping units consist of n cells connected in parallel to the same anode potential (Fig.5). Thus

$$S_n = n \, S_l \qquad (16)$$

where S_n is the pumping speed of the n cells.

This pumping speed is lowered to S_{eff} due to the conductance of the slits between the anode and the two cathodes [1,13].

$$S_{eff} = S_n \frac{\tanh D}{D} \qquad (17)$$

with $$D = \frac{ka}{7{,}85 \, \delta} \sqrt{\frac{S_n}{ab}}$$

where

- a = depth of a pumping unit in cm.
- b = length of the pumping unit in cm.

k = factor taking the value 1 when the pumping unit is open to one side and the value $\frac{1}{2}$ for two open sides.

δ = the gap between anode and one cathode in cm (Fig.5).

If the sputter-ion pump consists of N pumping units, the effective pumping speed on the pump flange S_p can be calculated by the equation:

$$\frac{1}{S_p} = \frac{1}{NS_{eff}} + \frac{1}{L} \qquad (18)$$

where L is the conductance of the pump chamber to the connecting flange.

The pumping speed S_p can be also calculated with more computational effort, using the matrix calculations [14] proposed by Pisani [15,16].

The equations (11), (12), (13), (14), (15), (16) and (17) can be also used for carbon monoxide.

The proposed formalism is not extended to inert gases and hydrogen due to the complicated pumping speed dependence on the cathode material [17,18].

The saturated pumping speed is needed in most practical cases for users and manufacturers of sputter-ion pumps. It is defined as the pumping speed after a quantity of $2 \cdot 10^{-2} \cdot S$ Torrlit gas has been pumped (S = nominal pumping speed in lit/sec)[19]. This saturation can for instance be achived by operating of the pump at $1 \cdot 10^{-6}$ Torr for 5,5 hours.

To calculate the saturated pumping speed, the equations (13),(14) and (15) must be multiplied by the factor $(0,75 - \frac{2 \cdot 10^{-10}}{p})$. This factor includes also the outgasing effects on the pumping speed.

Using the proposed formalism the pumping speed of the prototypes of distributed sputter-ion pumps of SPEAR [2] was calculated at $5 \cdot 10^{-7}$ Torr and plotted together with the measured values in Fig. 1. The good agreement can be observed. The existing deviation of 25 % for the Ø 1,25 cm cells at high magnetic fields lies within the accuracy of the pumping speed measurements. In another publication of the

SPEAR-group [20] the max. pumping speed of the Ø 1,25 cm elements is rated with 500 lit/sec. This value is close to our calculations.

Two other numerical applications of the formalism are demonstrated in Fig.6 and Fig.7 for two conventional pumps rated at 400 lit/sec. Pump I (Fig.6) has been installed as standard sputter-ion pump in the vacuum system of the DORIS storage ring.

The pump parameters have the following values:

	Pump I	Pump II
N	4 elements	16 elements
L	1200 lit/sec	1200 lit/sec
n	123 cells/element	8 cells/element
r_a	1,03 cm	1,25 cm
ℓ_a	2,54 cm	2,0 cm
δ	1,22 cm	0,8 cm
a	13,3 cm	7 cm
b	43 cm	10,6 cm
B	1090 G	1000 G
U_a	5000 V	7500 V

Both pumps are working in the LMF-mode up to 10^{-6} Torr. In this case, the pumping speed depends on the value of magnetic field ($\propto B^2$). To avoid deviations, due to different magnetic field values at different cells, the mean square root of the magnetic field over the whole surface of the element was taken into account.

The agreement between calculated and measured values - depending on the accuracy of the pumping speed measurements - is better than 30 %.

Equation (17) was used for conductance corrections in the pump elements in all numerical applications. The corrections was always less than 25 % of the pumping speed of an element.

References:

1) M.D.Malev and E.M.Trakhtenberg, Preprint 280, Inst.Nucl.Phys.Novosibirsk,1969.

2) U.Cummings et al, J.Vac.Sci.Technol.,8, 348(1971).

3) V.V.Ryabov and G.L.Saksagansky, Vacuum, 22, 191(1971).

4) Vorschlag zum Bau eines 3 GeV Elektron-Positron-Doppelspeicherringes für das Deutsche Elektronen-Synchrotron, (DESY,Hamburg,1967), p.55.

5) M.Bernardini and L.Malter, J.Vac.Sci.Technol.,2, 130(1965).

6) W.Schuurman, Invest.of a Low-Pressure Penning Discharge,Rijnhuizen Report 66-28 (FOM-Instituut voor Plasma-Fysica, Rijnhuizen, Netherlands,1966).

7) W.Bächler, Third Int.Vac.Congr. Stuttgart, 2, 609(1967).

8) R.L.Jepsen Le Vide 80, 80, (1959).

9) S.L.Rutherford, Trans. 10th AVS Vacuum Symposium, 185(1963).

10) A.Dallos and F.Steinrisser, J.Vac.Sci. Technol. 4, 6(1967).

11) A.Dallos Vacuum, 14, 79(1969).

12) E.Fischer, H.Mommsen, ISR-VAC/66-11(CERN,1966).

13) G.A. Vasil'ev, Pribori i Technika Eksperimenta, 147(1965).

14) G.Paul, Vakuum Technik, 22, 243(1973).

15) C.Pisani, Vacuum, 18, 327(1968).

16) C.Pisani, Proc. 4th Intern.Vacuum Congr.,439(1968).

17) P.N.Baker and L.Laurenson, J.Vac.Sci. Technol. 9, 375(1972).

18) J.H.Singleton, J.Vac.Sc. Technol. 6, 316(1969).

19) ISO-Proposal, (ISO/TC112/SC3, 1970).

20) B.Richter, Kerntechnik, 12, 531(1970).

21) M.D.Malev and E.M.Trakhtenberg, Vacuum, 23, 403(1973).

Acknowledgements

The authors are indebted to D. Degèle, J. Susta and K. Steffen for helpful suggestions and to J. Lehmitz and M.G. Meczulat for their skillful technical assistence on pumping speed measurements.

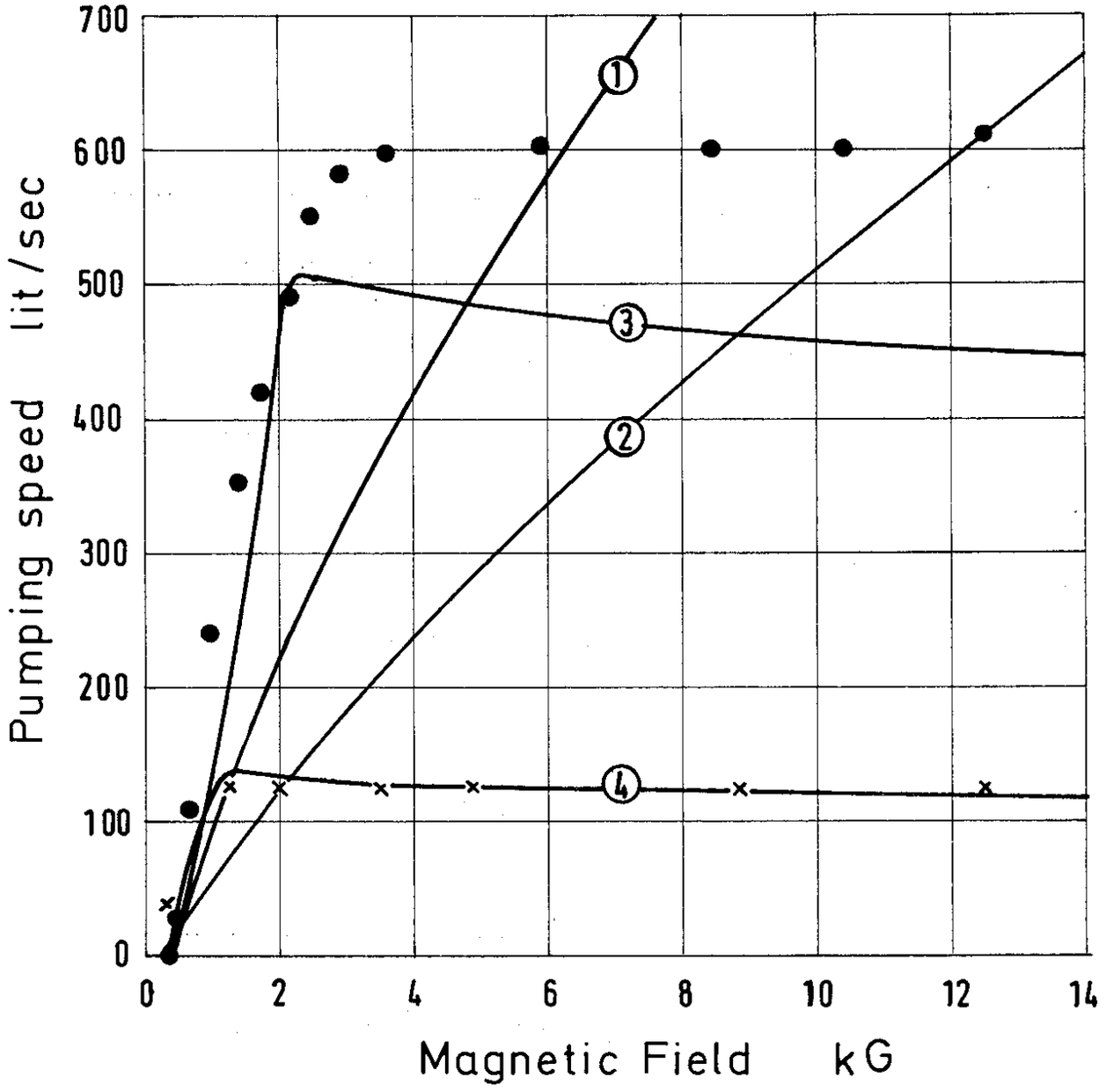

Fig. 1: Pumping speeds of SPEAR storage ring pumps.

● measured values with 1,25 cm diam. cells
× " " " 2,50 cm " "
① calc. pumping speed with Malev's formalism[1] for 1,25 cm diam. cells
② " " " " " " 2,50 cm " "
③ " " " as proposed in this paper" 1,25 cm " "
④ " " " " " " 2,50 cm " "

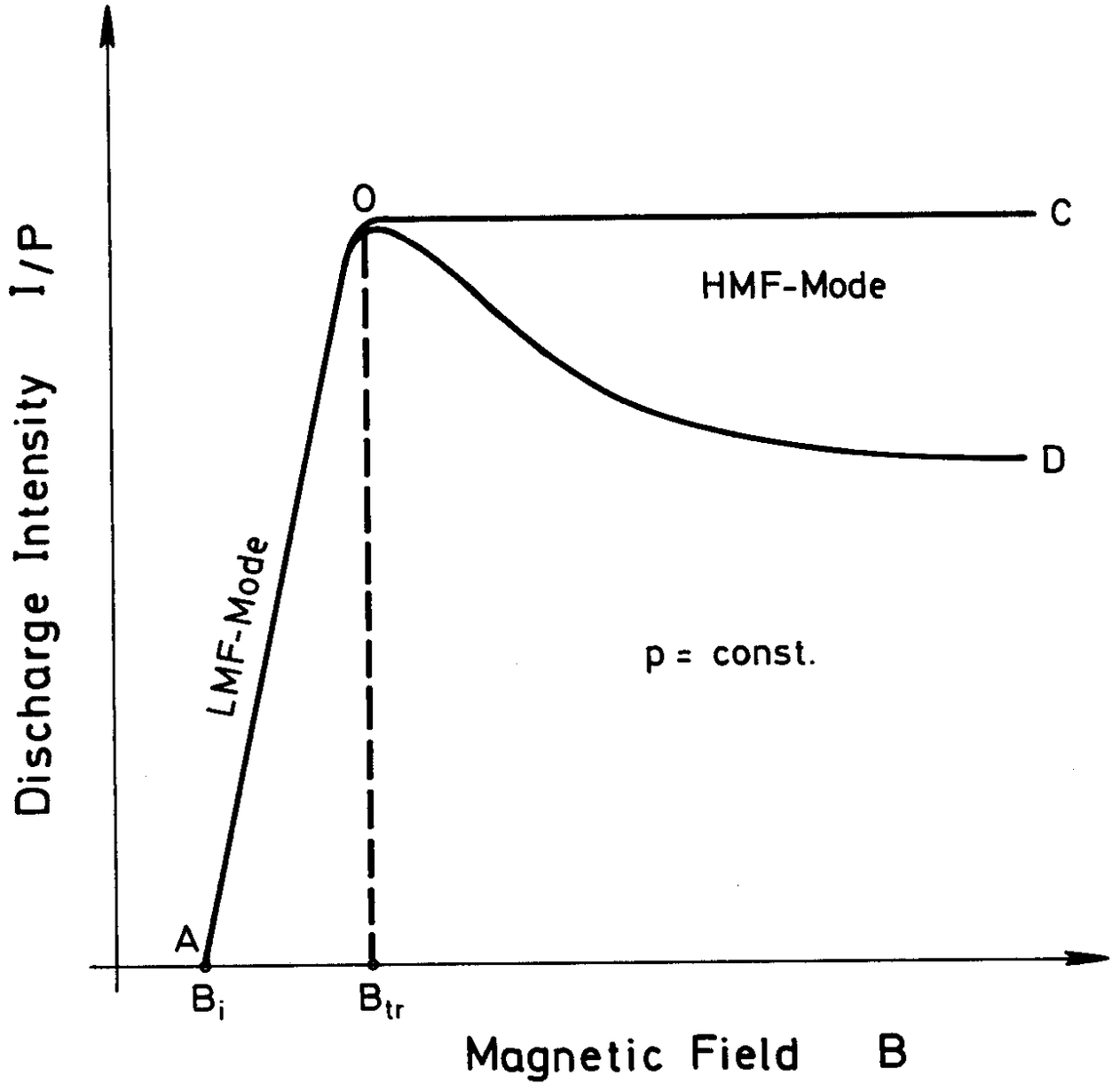

Fig. 2: A typical diagram of the discharge intensity dependence on the magnetic field at constant pressure. The brance AO is characteristic for the LMF-mode. At low pressures ($p < 10^{-7}$ Torr) the HMF-mode (oc) shows an almost constant discharge intensity. For high pressures ($p > 10^{-7}$ Torr) the HMF-mode is given by the curve OD.

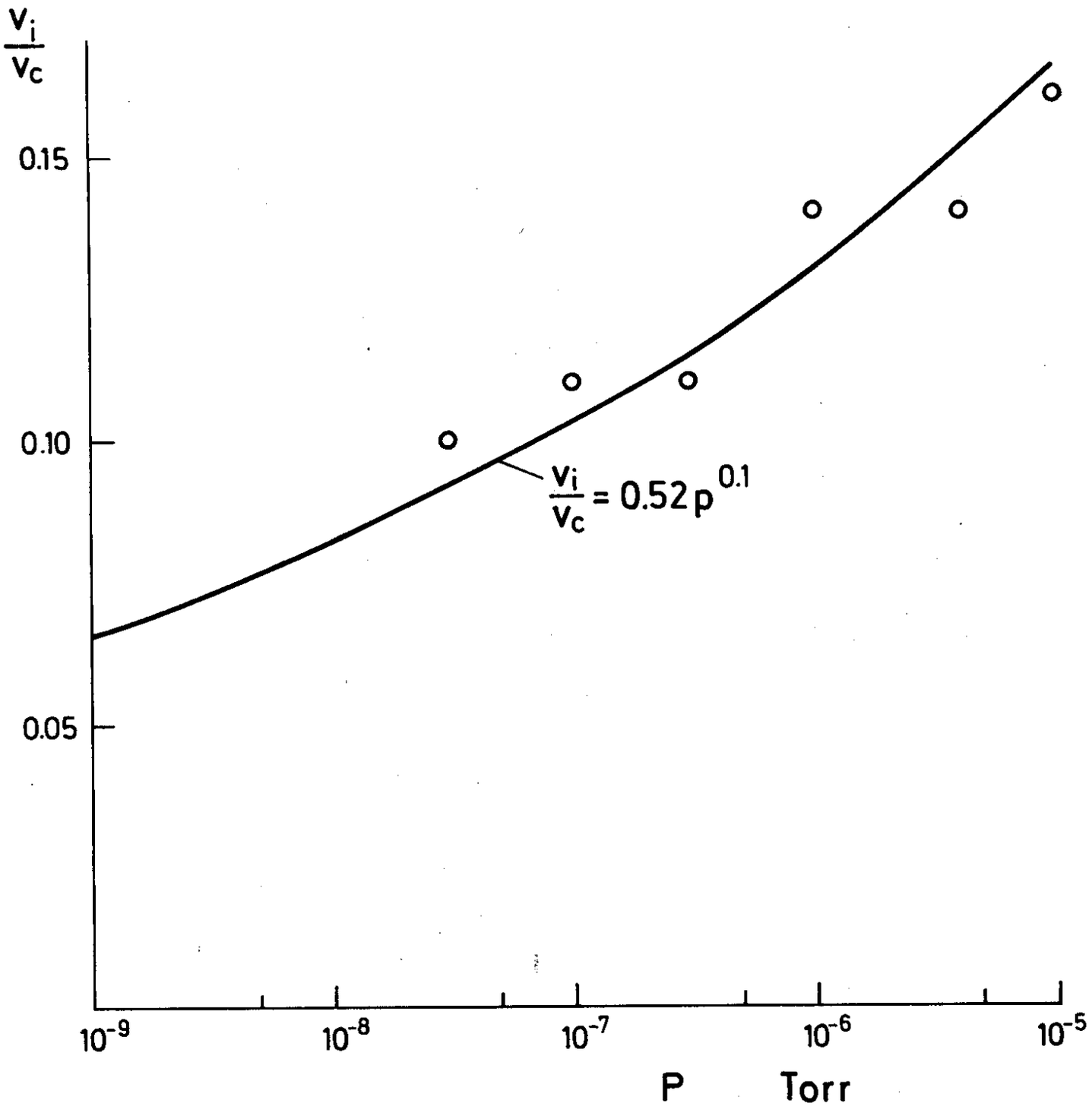

Fig. 3: Measured [6] and proposed pressure dependence of the ionization probability $\frac{\nu_i}{\nu_c}$.

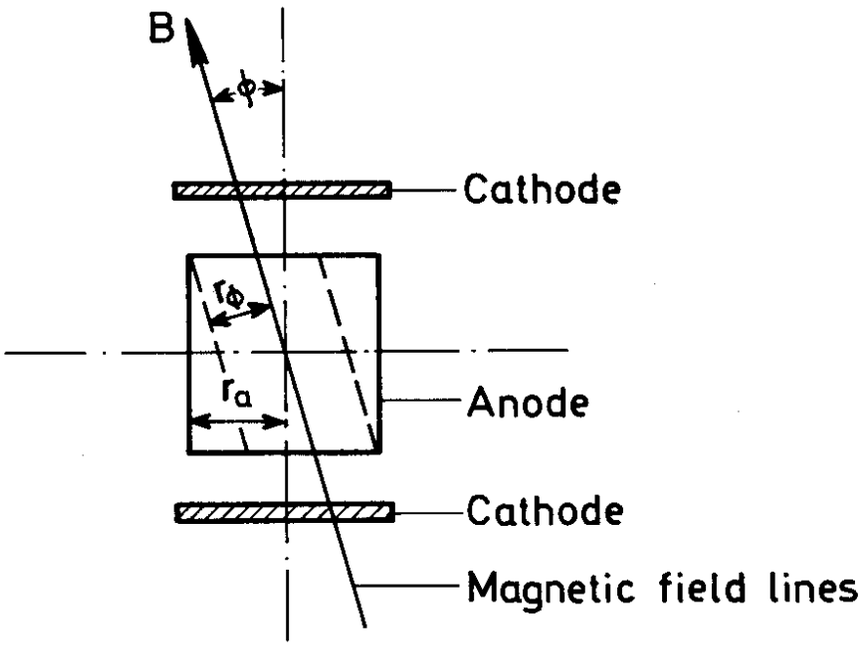

Fig. 4: The decrease of the effective cell radius due to misalignment of cell axis to magnetic field.

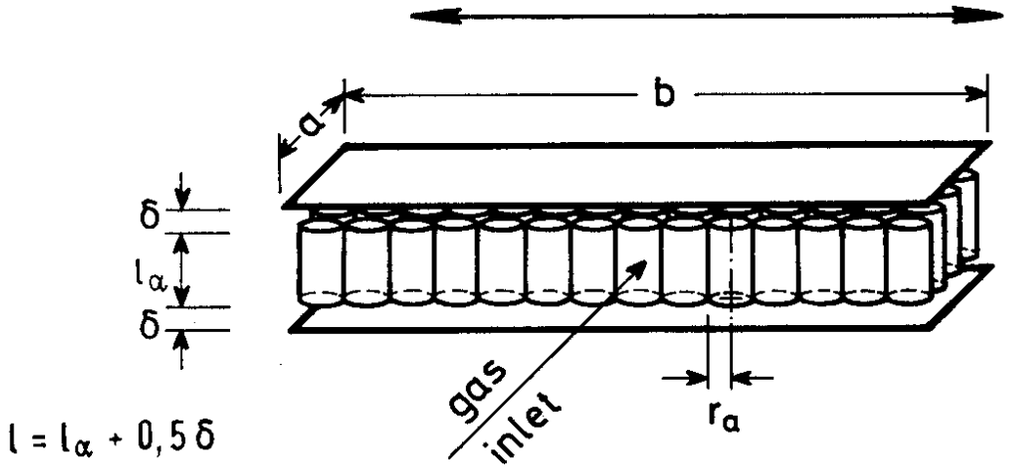

Fig. 5: Electrode structure of a sputter-ion pump element and its characteristic dimensions.

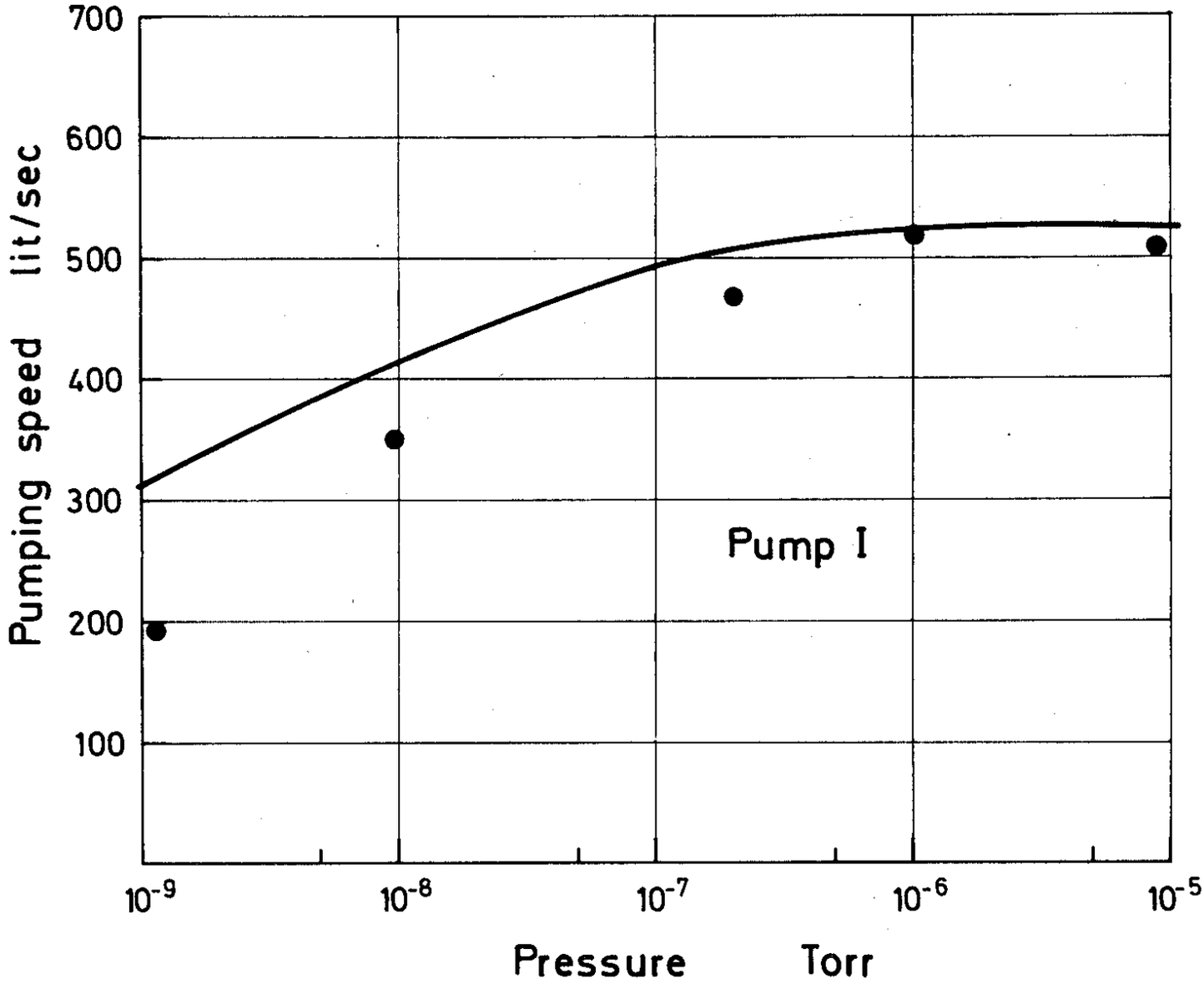

Fig. 6: The pumping speed pressure dependence of the 400 lit/sec conventional sputter-ion pumps, installed in the vacuum system of DORIS.

● measured not saturated pumping speed,

— calculated pumping speed as proposed in this work.

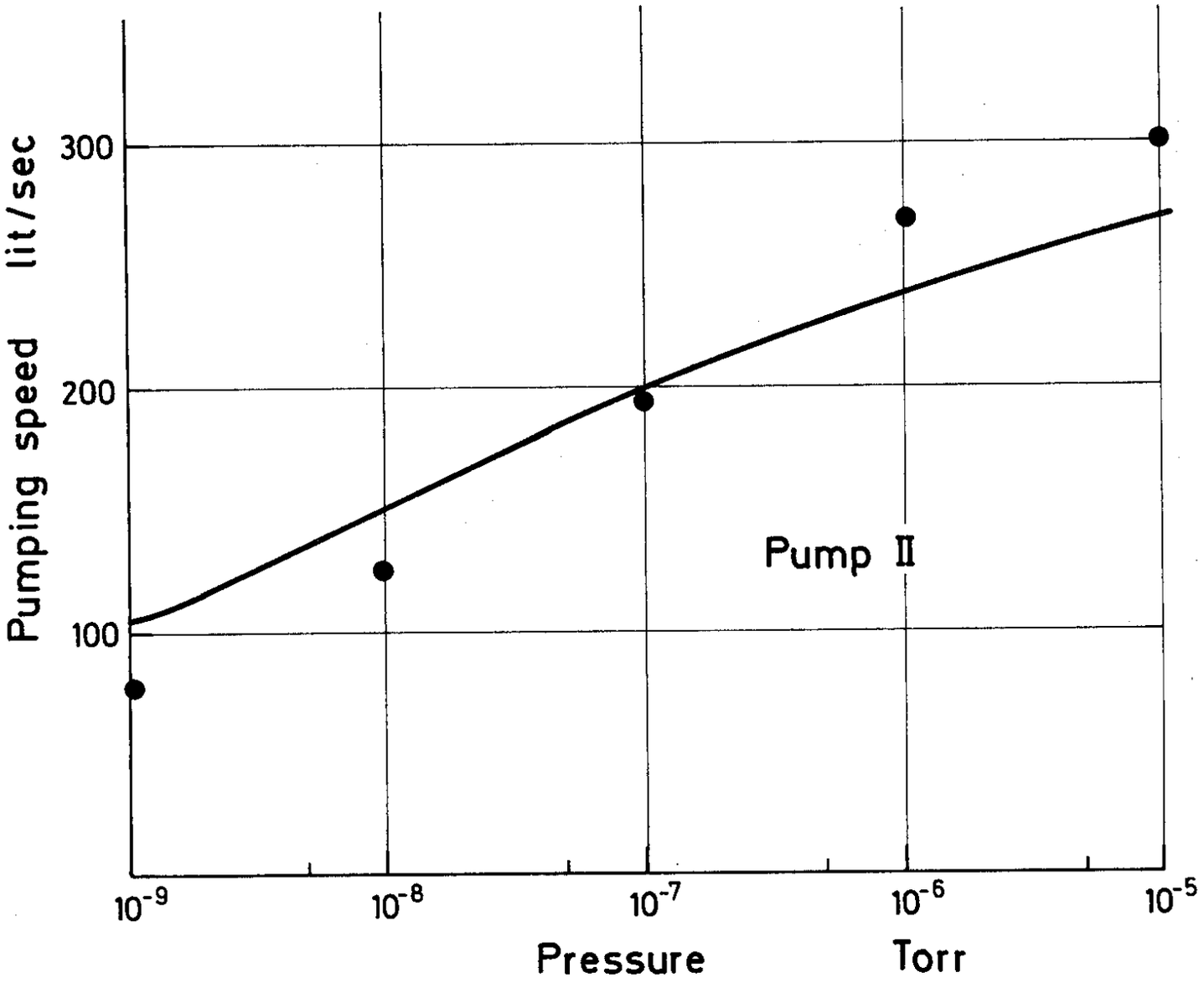

Fig. 7: The pumping speed pressure dependence of a conventional sputter-ion pump (II).

● measured not saturated pumping speed

— calculated pumping speed as proposed in this work.